01 Oct 1999

Doppler Shift Anisotropy in Small Angle Neutron Scattering

Barbara Ellen Wyslouzil

Gerald Wilemski
Missouri University of Science and Technology, wilemski@mst.edu

Janice L. Cheung

Reinhard Strey

et. al. For a complete list of authors, see https://scholarsmine.mst.edu/phys_facwork/1201

Recommended Citation

B. E. Wyslouzil et al., "Doppler Shift Anisotropy in Small Angle Neutron Scattering," *Physical review. E, Statistical physics, plasmas, fluids, and related interdisciplinary topics*, vol. 60, no. 4 B, pp. 4330-4335, American Physical Society (APS), Oct 1999.
The definitive version is available at https://doi.org/10.1103/PhysRevE.60.4330

Doppler shift anisotropy in small angle neutron scattering

B. E. Wyslouzil,[1] G. Wilemski,[2] J. L. Cheung,[1] R. Strey,[3] and J. Barker[4]
[1]*Department of Chemical Engineering, Worcester Polytechnic Institute, Worcester, Massachusetts 01609*
[2]*Department of Physics and Cloud and Aerosol Sciences Laboratory, University of Missouri-Rolla, Rolla, Missouri 65409*
[3]*Institut für Physikalische Chemie, Universität zu Köln, D-50939 Köln, Germany*
[4]*Cold Neutron Research Facility, National Institute of Standards and Technology, Gaithersburg, Maryland 20899*
(Received 16 March 1999)

The two-dimensional patterns in our small angle neutron scattering (SANS) experiments from rapidly moving aerosols are anisotropic. To test the kinematic theory of two-body scattering that describes the anisotropy, we conducted SANS experiments using a constant source of D_2O aerosol with droplets moving at $\sim$440 m/s, and varied the neutron velocity from 267 to 800 m/s. The theoretically predicted anisotropy of the laboratory scattering intensities agrees well with the experimental results. Based on an analysis of the scattering intensity in the Guinier region, we also determined the particle velocity. The results are in very good agreement with independent velocity estimates based on supersonic flow measurements.
[S1063-651X(99)02310-7]

PACS number(s): 61.12.Ex, 82.70.Rr, 64.70.Fx, 47.40.Ki

I. INTRODUCTION

We recently reported the first small angle neutron scattering (SANS) measurements for aerosols formed in a supersonic nozzle [1]. These crossed-beam scattering measurements contain much valuable information about the size distribution of the particles formed by nucleation and condensational growth during the rapid gas expansion. Extracting this information requires a very careful data analysis, which is complicated by the relative motion of the neutrons and aerosol particles. Because of the directed motion of the aerosol particles, the measured laboratory scattering patterns are anisotropic. Neutrons scattered with a momentum component along or against the direction of particle motion incur larger momentum transfers than those scattered orthogonally to it. As a result, laboratory scattering intensity falls off faster along the axis of particle motion than normal to it. In effect, the momentum of the scattered neutrons is Doppler shifted. As shown later, this Doppler shift can be used to directly measure the particle speed.

In our first experiments [1] the velocity of the neutrons v_n was fixed at 800 m/s, which is about two times the velocity of the aerosol particles v_p. The anisotropy due to the Doppler shift, although clearly present, was not large. In order to test our understanding of this effect more stringently, we conducted a series of experiments in which aerosol was continuously produced under constant conditions and the scattering patterns were measured for different neutron speeds. In all, the average value of v_p/v_n covered the range 0.55 to 1.65.

In this paper, we analyze the results of these experiments using the theoretical framework presented in detail elsewhere [2]. We show that the experimental results are in full accord with theoretical expectations. Moreover, we take advantage of the anisotropy of the scattering pattern as reflected in the slopes of different types of Guinier plots to deduce the velocity of the aerosol particles. The results are in very good agreement with independent velocity estimates based on pressure trace measurements.

Section II summarizes the key equations relating to the laboratory and center-of-mass scattering intensities. These equations also provide the basis for determining the aerosol particle speed by a Guinier analysis of the scattering intensities. In Sec. III we describe the experiments and present the experimental data that clearly demonstrate the anisotropy of the scattering patterns and validate the theory presented in Sec. II. A summary of the results and the conclusions are given in Sec. IV.

II. THEORY

As shown elsewhere [2] for the right angle crossed beam geometry of our experiment (see Fig. 1), the laboratory scattering intensity I is related to the scattering intensity I_0 in the center-of-mass frame by the equation

$$I(q)=I_0(q_0)\frac{(\xi+\sqrt{1+\xi^2})^2}{\sqrt{1+\xi^2}}, \tag{2.1}$$

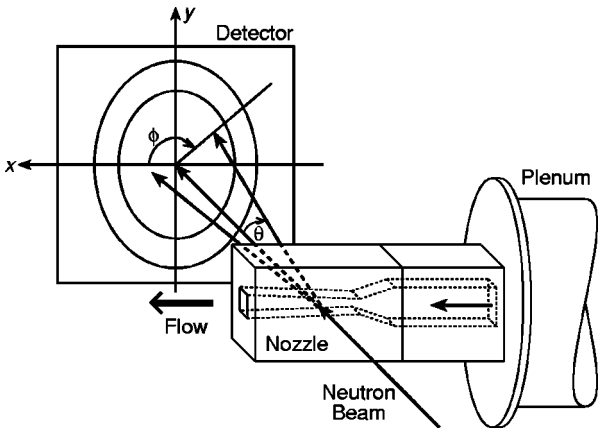

FIG. 1. The aerosol is formed in the nozzle upstream of the viewing volume. The neutron beam passes through the sample at right angles to the flowing aerosol. The laboratory scattering angles θ and ϕ are defined, and two contour lines of constant scattering intensity are shown on the detector.

where

$$\xi=(v_p/v_n)\sin\theta\cos\phi, \tag{2.2}$$

θ is the usual laboratory scattering angle and ϕ is the azimuthal scattering angle measured in the detector plane. The momentum transfer wave vectors, q and q_0, in the respective laboratory and center-of-mass frames, are equal and are expressed in laboratory variables as

$$q^2=q_0^2=2k^2[1+(\xi-\cos\theta)(\xi+\sqrt{1+\xi^2})], \tag{2.3}$$

where the incident neutron wave vector k is related to the neutron wavelength λ in the usual way,

$$k=2\pi/\lambda. \tag{2.4}$$

Equations (2.1)–(2.3) are valid for the elastic scattering of neutrons by very massive aerosol particles.

Since the total volume fraction of aerosol particles is $<10^{-5}$, multiple scattering is negligible. Interparticle correlations may also be neglected because the aerosols are dilute. Thus, for a distribution of different sized particles, I_0 can be theoretically determined by summing the contributions from individual particles,

$$I_0(q)=\sum_j N(r_j)P(q,r_j), \tag{2.5}$$

where $N(r_j)$ is the number density of paricles with radius r_j. For a spherical aerosol particle of uniform composition, the particle form factor [3] $P(q,r)$ is

$$P(q,r)=16\pi^2(\rho_b)^2(\sin qr-qr\cos qr)^2/q^6, \tag{2.6}$$

where ρ_b is the scattering length density of the particle.

These equations form the basis for the data analysis algorithm described in the following section. An important component of this algorithm is a Guinier analysis of the small q behavior of $I(q)$. Since q itself depends on the as yet unknown particle velocity, it is not a useful plotting parameter, but for small θ Eq. (2.3) reduces to

$$q^2=q_i^2[1+\xi+(v_p/v_n)^2\cos^2\phi], \tag{2.7}$$

where q_i is the nominal momentum transfer wave vector based on the incident (i) neutron wavelength,

$$q_i=(4\pi/\lambda)\sin(\theta/2). \tag{2.8}$$

Since q_i is independent of v_p, the Guinier analysis can be carried out by plotting the logarithm of suitably averaged values of $I(q)$ versus q_i^2. The equations [2] needed to theoretically interpret these plots are found by expanding Eqs. (2.1) and (2.6) to second order in q and ξ,

$$I(q)=I(0)[1-q^2r_G^2/3][1+2\xi+3\xi^2/2], \tag{2.9}$$

followed by averaging with respect to ϕ. In Eq. (2.9), $I(0)$ is the scattering intensity at $q=0$, $I(0)=(4\pi\rho_b/3)^2N\langle r^6\rangle$, r_G is the radius of gyration, $r_G^2=(3/5)\langle r^8\rangle/\langle r^6\rangle$, N is the total number density of aerosol particles, and the mean values are defined as $N\langle r^n\rangle=\Sigma_j(r_j)^nN(r_j)$. Here, we consider three types of averages. The results are valid for $r_G^2\gg\lambda^2$.

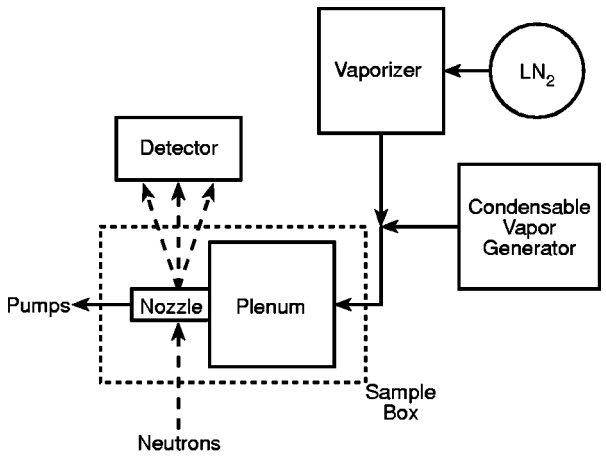

FIG. 2. A schematic diagram of the experimental setup.

First, we take a circular average of $I(q)$ over the azimuthal angle ϕ at constant θ (or q_i). We denote the result as $\overline{I_c}(q_i)$ and expand its natural logarithm to obtain

$$\ln\overline{I_c}(q_i)=\ln I(0)-q_i^2r_G^2[1+\tfrac{1}{2}(v_p/v_n)^2]/3. \tag{2.10}$$

Next, we take a ''horizontal'' average, denoted as $\overline{I_h}$, by averaging pairs of intensities at $\phi=0$ and π to find

$$\ln\overline{I_h}(q_i)=\ln I(0)-q_i^2r_G^2[1+(v_p/v_n)^2]/3. \tag{2.11}$$

Finally, we take a similar ''vertical'' average, denoted as $\overline{I_v}$, by averaging pairs of intensities at $\phi=\pm\pi/2$ to find

$$\ln\overline{I_v}(q_i)=\ln I(0)-q_i^2r_G^2/3. \tag{2.12}$$

These results show that the velocity dependence of the apparent Guinier slope depends on the type of average taken. By taking a ratio of the values of these slopes it is possible to determine, by direct experimental means, the particle velocity, as will be demonstrated shortly. In our experiments, the particle velocity varies along the field of view, and contributions to $I(q)$ arise from different particle velocities. In this case, v_p^2 in the above equations should be replaced by its average along the flow field, which can be written as $\overline{v_p}^2[1-\frac{1}{12}(\Delta v_p/\overline{v_p})^2]$, where $\overline{v_p}$ is the average particle velocity and Δv_p is the difference between the maximum and minimum values of v_p at the boundaries of the field of view. For the current conditions, this correction is entirely negligible, and $\overline{v_p^2}=\overline{v_p}^2$.

III. SANS EXPERIMENTS

A. Equipment and facilities

A schematic diagram of the experimental setup used to generate the aerosol and perform the SANS measurements is illustrated in Fig. 2. The key components of the apparatus, described in more detail in separate publications [1,4] include (i) the carrier gas generator, (ii) the condensible vapor generators, and (iii) the supersonic nozzle. To summarize, a carrier gas (N_2) containing ~1% to 2% by weight of a condensible vapor flows through a gently diverging two-dimensional Laval nozzle. As the gas expands and cools, the

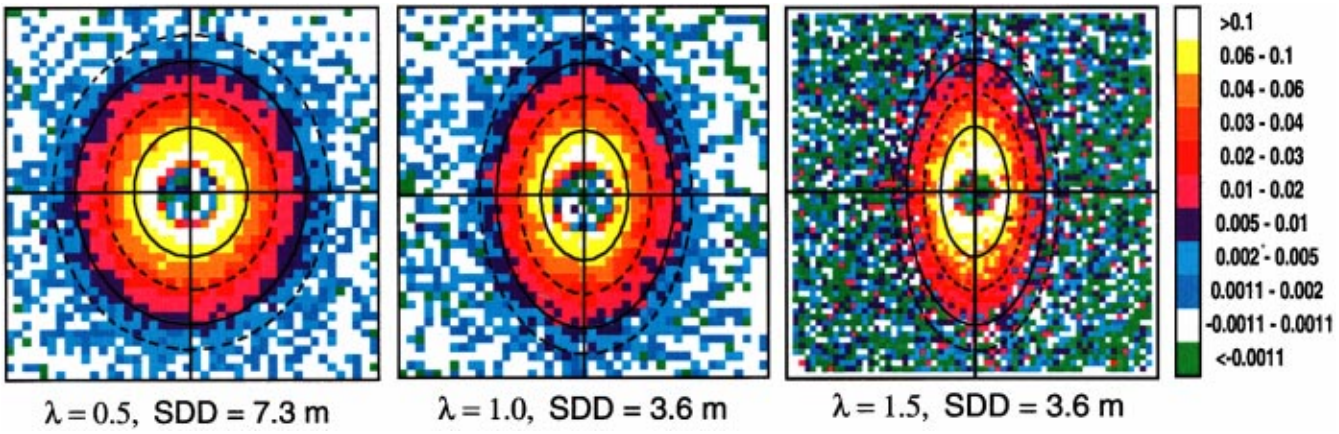

FIG. 3. (Color) The nearly elliptical two-dimensional scattering patterns for a nanodroplet aerosol moving at ~440 m/s become progressively more eccentric as the neutron wavelength is changed from 0.5 to 1.5 nm. Each colored square corresponds to one of the 1 cm $\times$1 cm elements on the detector. The color bar at the right gives the absolute signal intensity in cm^{-1}. The images have been cropped and rescaled so that the axes cover the same range of q_i. The contours were calculated using Eqs. (2.1)–(2.6), the best fit parameters for the size distribution of the aerosol, $\langle r \rangle = 9.8$ nm, $\sigma_r = 3.45$ nm, $N = 3.6 \times 10^{11}\,cm^{-3}$, and a particle velocity of 440 m/s. The innermost solid contour corresponds to an absolute intensity of $0.08\,cm^{-1}$. The three other contours are at 0.03, 0.008, and $0.003\,cm^{-1}$, respectively.

supersaturation of the condensible vapor increases until a point is reached where rapid particle formation and particle growth deplete the vapor and reduce the supersaturation to close to 1. Under typical operating conditions, the particle number concentration is on the order of $10^{12}\,cm^{-3}$ and the average particle radius is in the range of 5 nm to 12 nm. Based on strong theoretical arguments, e.g., Schwartz and Andres [5] and as shown experimentally below, the particles are moving at the same speed as the gas. As illustrated in Fig. 1, the velocity is in the direction of the x axis. The gentle divergence of the nozzle ensures that the velocity component in the y direction is essentially zero and the parallel side walls provide a constant neutron pathlength through the sample. The side walls of the nozzle contain silicon windows that are transparent to the neutrons. The key challenge in designing the equipment is to produce a stable aerosol for the extended periods of time required to get good SANS signals despite stopping and restarting the equipment many times over the course of several days of beam time. Strong evidence of this capability will be given below, and additional proof that the experimental setup is extremely reliable is presented elsewhere [4]. Because the experiments are conducted at the National Institute of Standards and Technology (NIST), the entire apparatus must be easy to break down, transport, and reassemble quickly.

The SANS experiments were conducted on different occasions using the NG7 beam line at NIST in Gaithersburg, Maryland. The plenum, flow straightener, and nozzle are located in a 1.1-m$\times$0.4-m$\times$0.6-m evacuated sample box. Removing the air greatly reduces the background scattering signal due to N_2, O_2, and H_2O vapor in the sample box and gives a more stable signal from both the ''empty'' nozzle and the nozzle with aerosol present. Because of the asymmetry in the two-dimensional scattering pattern that is the focus of this paper, we work exclusively with the beam centered on the detector.

B. Results, data analysis, and discussion

The goal of these experiments was to stringently test the theoretical predictions presented in Sec. II. From Eqs. (2.1)–(2.3), the degree of anisotropy in the two-dimensional small-angle scattering pattern is a strong function of v_p/v_n because both the intensity and q depend on it. One direct way to test the predicted dependence on v_p/v_n is to change the neutron wavelength and, hence, the neutron speed, while maintaining stable conditions for particle formation in the nozzle to keep v_p unchanged. Unless otherwise noted, all experiments were conducted using a stagnation pressure p_0 of 60 kPa, a condensible vapor pressure p_v of 1.4 kPa of D_2O and a stagnation temperature T_0 of 304 K. Under these conditions, an analysis of the pressure traces for the condensing and dry flows gives a gas velocity that ranges from 416 to 458 m/s in the observation region. At the neutron-scattering facility at NIST, neutrons can be selected in the range of 0.5 nm to 2.0 nm. This study used neutron wavelengths of 0.5 nm, 0.6 nm, 1.0 nm, and 1.5 nm which correspond to v_n values of 800 m/s, 667 m/s, 400 m/s, and 267 m/s, respectively.

Figure 3 illustrates the two-dimensional scattering patterns that were observed when we varied the neutron wavelength while maintaining constant aerosol formation conditions. As in Figs. 1 and 2, the particles were moving from right to left. The position of the detector was changed from 7.3 m at $\lambda_n = 0.5$ nm to 3.6 m for $\lambda_n = 1.0$ nm and 1.5 nm in order to maintain about the same range of q_i. At $\lambda = 1.0$ nm we also made measurements at a sample to detector distance of 5.5 m in order to extend the range of q to lower values. In Fig. 3, only the data at 3.6 m are shown. As predicted by the theory, the scattering patterns are nearly elliptical in shape, and they change from nearly circular to highly eccentric as the neutron wavelength changes from 0.5 nm to 1.5 nm.

The scattering patterns presented in Fig. 3 were generated in the following manner. The raw scattering signal from the aerosol was corrected by subtracting the scattering signal from the nozzle flowing pure N_2. In our case, because the transmission of the sample T_{sam} equals the transmission of the empty cell T_{emp} and both are very close to 1, the correction step is simplified because any effect of the beam-blocked component of the background cancels. The cor-

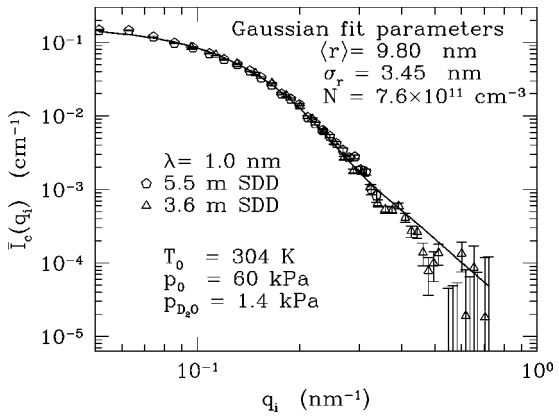

FIG. 4. The circularly averaged intensity is plotted as a function of q_i. The measurements were made at $\lambda = 1$ nm and two sample to detector distances (SDD). An incoherent background of $2.4 \times 10^{-4}\,\mathrm{cm}^{-1}$ has been subtracted from the 3.6-m data. The solid line is the predicted scattering intensity for an aerosol moving at 440 m/s. The best fit values for $\langle r \rangle$, N, and σ_r, for a Gaussian size distribution, are given in the figure.

rected data set was then adjusted for any nonuniformities in the detector efficiency by dividing the intensities by the measured scattering intensity from a water sample on a pixel-by-pixel basis. The data were then placed on an absolute scale and standard masking of the bad areas of the detector was applied. The absolute scales were determined either by measuring the scattering from a standard sample (NIST A2 Silica Standard) under the same conditions used to measure the data, or by measuring the attenuated neutron flux reaching the detector during a beam center determination (direct beam measurement).

To quantitatively demonstrate that the observed scaling agrees with the theoretical predictions, we must determine the number density, the average particle size, and the width of the size distribution. The first step is to combine the 3.6-m and 5.5-m data sets available for $\lambda = 1.0$ nm in order to extend the scattering spectrum over as wide a q range as possible. The two data sets are plotted in Fig. 4 as the circularly averaged scattering intensities $\overline{I_c}$ against q_i. The values in Fig. 4 were generated from the two-dimensional scattering patterns using the AVERAGE command in the standard NIST data reduction package [6]. The error bars on this graph and all other graphs in this paper represent one standard deviation from the mean. Noisy data points in the high q portion of the 5.5 m data have been removed, and an incoherent backgound of $2.5 \times 10^{-4}\,\mathrm{cm}^{-1}$ has been subtracted from the 3.6-m data to extend the high q range. The agreement between the two data sets in the region of overlap is excellent especially considering that the scaling factors for the data sets were determined independently without any empirical adjustments. Furthermore, the scale factor at 3.6 m was determined from a direct beam measurement while at 5.5 m we measured the scattering from the A2 silica standard. Figure 4 clearly demonstrates that we are able to reliably reproduce the aerosol despite interrupting the experiment to change the SANS instrument setup.

To determine the best-fit parameters of the aerosol size distribution, we generated synthetic scattering patterns using Eqs. (2.1)–(2.6) for a Gaussian size distribution of droplets moving at the average velocity in the viewing volume 440 m/s. We systematically varied the values of the mean droplet diameter $\langle r \rangle$ and the width of the droplet distribution σ_r, calculated the scattering intensities averaged over ϕ at constant θ for an aerosol with these parameters, and optimized the droplet number concentration for each pair of trial values. Because the scattering intensity is directly proportional to the droplet number density, the chi-square quantity [7] involving the differences between values on the synthetic scattering curve and the data points can be written as

$$\chi^2 = \sum_{i=1}^{n} \frac{[N\overline{I_s}(q_i) - \overline{I_c}(q_i)]^2}{\sigma^2(q_i)}, \tag{3.1}$$

where $\overline{I_s}(q_i)$ is the synthetic scattering intensity for the droplet distribution with a number density of 1 cm^{-3} and $\sigma(q_i)$ is the uncertainty associated with the experimental value of $\overline{I_c}(q_i)$. Explicitly, $\overline{I_s}(q_i)$ is given by

$$\overline{I_s}(q_i) = \frac{1}{\sigma_r \sqrt{(2\pi)^3}} \int_0^\infty \int_0^{2\pi} \exp\left[-\frac{(r - \langle r \rangle)^2}{2\sigma_r^2} \right] P(q,r)\, d\phi\, dr, \tag{3.2}$$

where $P(q,r)$ comes from Eq. (2.6) and the ϕ dependence of q is given by Eqs. (2.2)–(2.4). It is easy to show that the value of N that minimizes χ^2 for each $\langle r \rangle$ and σ_r pair is given by

$$N = \frac{\Sigma_i \overline{I_s}(q_i)\overline{I_c}(q_i)/\sigma^2(q_i)}{\Sigma_i [\overline{I_s}(q_i)/\sigma(q_i)]^2}. \tag{3.3}$$

The best-fit values of $\langle r \rangle$, σ_r, and N were those that minimized χ^2 for $q_i \leqslant 0.514\,\mathrm{nm}^{-1}$. The solid line in Fig. 4 is the best-fit curve for the parameters found by this method, extended to cover the entire range of available data.

With the best fit parameters for the aerosol in hand, it is easy to calculate the expected two-dimensional scattering patterns as a function of wavelength and sample-to-detector distance using Eqs. (2.1) and (2.3). The solid and dashed lines in Fig. 3 are contours of constant absolute intensity that were generated using the appropriate parameters for the aerosol size distribution and the experimental setup. It is not too surprising that the agreement for $\lambda = 1$ nm is good since these data were used to derive the properties of the aerosol size distribution. However, the good fit of the anisotropy is an independent confirmation of the ϕ dependence of the theory because only circularly averaged data were used to determine the aerosol properties. The fact that the good agreement is maintained for the other two data sets at different wavelengths, sample-to-detector distances, and independently derived absolute intensity scale factors, confirms that we understand the anisotropy quantitatively, as well as qualitatively. It also shows that we are able to maintain stable aerosol production over the long periods of time (30–90 min) needed to gather the data.

Another way to test the data quantitatively is to average the two-dimensional scattering patterns in three ways at each wavelength: the usual circular average, an average over 15° sectors centered along the horizontal axis, and an average

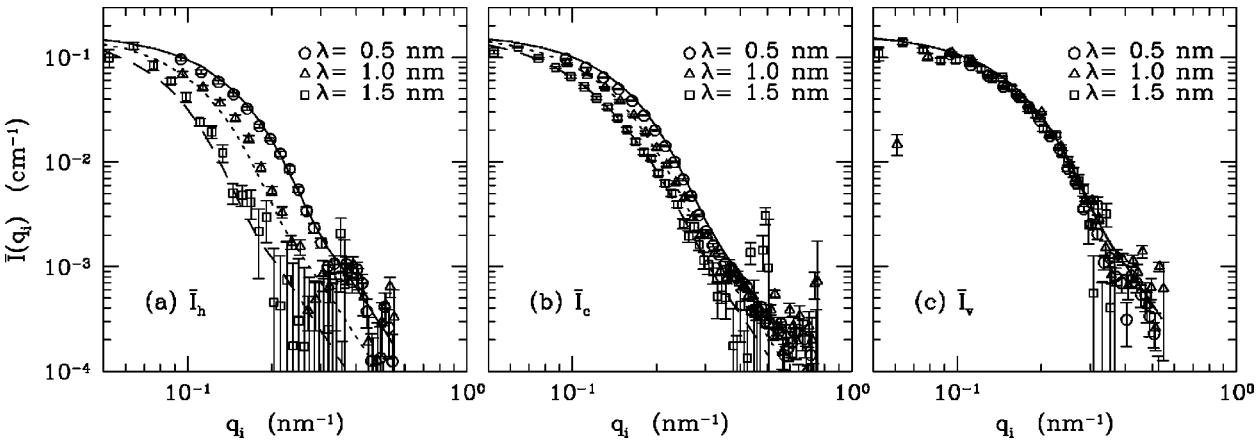

FIG. 5. Scattering spectra are derived from the two-dimensional data by averaging (a) across 15° segments along the horizontal axis, (b) along circles of constant radius, and (c) across 15° segments along the vertical axis. The lines correspond to the predicted intensities calculated using the derived particle size parameters.

over 15° sectors centered along the vertical axis. In the absence of flow, the scattering spectra should coincide independent of the averaging procedure or the wavelength. In our flow geometry (see Fig. 1), droplets have no significant momentum in the vertical direction, and the three ''vertical'' scattering spectra should collapse onto one curve. In contrast, the three ''horizontal'' scattering spectra should differ the most, and finally the circular averages should lie in between. Figure 5 compares the different spectra at the three neutron wavelengths, with all of the data placed on an absolute scale. The larger error bars associated with measurements at longer wavelength are due to two effects. The first is the decrease in the available neutron flux as λ is increased at a constant detector position. The second arises from analyzing the nearly elliptical scattering pattern with the circular averaging program (AVERAGE) that misinterprets the regular oscillations as an error (see Fig. 3 in Ref. [1]). In addition, the data in Fig. 5 appear to cover a smaller absolute intensity range than those presented in Fig. 4. This is primarily because the 15° sector averages use only about 10% of the available detector signal. Thus, at higher q the signal is not stable enough to let us estimate a reasonable value for the incoherent background in order to extend the range of the data as we did in Fig. 4. In spite of these difficulties, the anticipated trends are reproduced rather well in Fig. 5, and the importance of the theoretical framework we have developed to interpret the scattering signals is clearly illustrated. The lines drawn through the data points are the predicted scattering intensities based on the droplet size distribution parameters derived above after integrating over the same sectors as for the data. Again, the agreement is quantitative for each of the averages at each wavelength.

When the data at low q are good enough, it is possible to use the anisotropy to extract the particle velocity directly. Because the scattering intensity along the vertical axis is not perturbed by the particle motion, the slope derived from a Guinier plot of the vertically averaged data is $-r_G^2/3$ [c.f. Eq. (2.12)]. Alternatively, from Eq. (2.10) we see that when the circularly averaged intensities are used in the Guinier plot, the slope equals $-r_G^2(1+\frac{1}{2}(v_p/v_n)^2)/3$, and from Eq. (2.11) when the horizontally averaged intensities are used, the Guinier slope is $-r_G^2(1+(v_p/v_n)^2)/3$. Thus within a given data set the ratios of the three slopes can be used to derive the particle velocity directly. Figure 6 illustrates the three different Guinier plots for experiments in which $\lambda = 0.6\,\mathrm{nm}$, $p_0 = 60\,\mathrm{kPa}$, $p_v = 1.15\,\mathrm{kPa}$, and $T_0 = 299\,\mathrm{K}$. The horizontal and vertical averages are again performed over sectors 15° wide. Similar sector averages of Eq. (2.9) result in coefficients that differ from the ''true'' values by less than 0.5%. Thus the slopes in these plots may be interpreted using Eqs. (2.11) and (2.12). Because the value of the Guinier slope varies slightly with the number of points used, the number of points in each fit was varied from 10–14. For each fit, the particle velocity was derived using the ratio of the horizontal/vertical, circular/vertical, and horizontal/circular Guinier slopes. For this data set, the average of the particle velocities derived from the ratios of the horizontal/vertical Guiner slopes was $v_p = 438 \pm 8$ m/s, from the ratios of circular/vertical slopes was $v_p = 436 \pm 7$ m/s, and from the ratios of the horizontal/circular slopes was $v_p = 442 \pm 24$ m/s. The error estimates for the velocities correspond to one standard deviation from the mean. The average veloci-

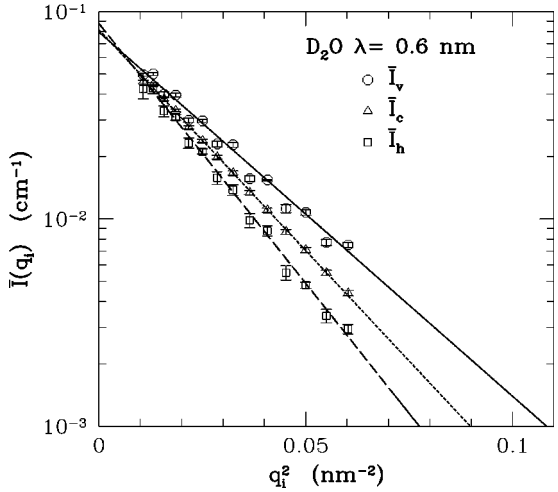

FIG. 6. The Guinier plots for the horizontal, circular, and vertical averages are shown along with the best-fit straight lines based on a weighted fit through the first 14 points. The corresponding values of the slopes are -57.77, -49.02, and $-40.44\,\mathrm{nm}^{-2}$, respectively.

ties are within 1% of the mean flow velocity, 440 m/s, expected in the viewing volume from the pressure trace data under these conditions. From Eqs. (2.10)–(2.12), the intercepts of the Guinier plots should also agree. In Fig. 6 the values of the individual intercepts differ by less than 5% from the mean.

IV. SUMMARY AND CONCLUSIONS

We tested the kinematic theory of two-body elastic scattering that describes the anisotropy in our two-dimensional SANS signals. The theory is the key to properly interpreting our experimental data and deriving accurate particle size distributions. Furthermore, with accurate scattering measurements in the low q region, we can use the anisotropy in the signal to measure the actual particle velocity. Our experiments using a fixed aerosol size distribution and variable neutron wavelength clearly demonstrate the validity of the theory and are an independent check of the stability of the aerosol.

ACKNOWLEDGMENTS

The assistance of our local NIST contact Dr. C. Glinka is gratefully acknowledged as is the help of Dr. Melissa Lunden and Mr. Chris Heath. This work was supported by the National Science Foundation, Division of Chemistry, under Grant Nos. CHE-9502604 (BEW), CHE-9522127 (BEW), and CHE-9729274 (BEW), by the Donors of the Petroleum Research Fund administered by the American Chemical Society, by NATO Travel Grants, and by the U.S. Department of Energy, Office of Basic Energy Sciences, Division of Geosciences and Engineering (GW). The work is based on activities supported by the National Science Foundation under Agreement No. DMR-9423101.

[1] B. E. Wyslouzil, J. L. Cheung, G. Wilemski, and R. Strey, Phys. Rev. Lett. **79**, 431 (1997).

[2] G. Wilemski, Phys. Rev. E (to be published).

[3] *Small Angle X-ray Scattering*, edited by O. Glatter and O. Kratky (Academic, London, 1982).

[4] B. E. Wyslouzil, C. H. Cheung, J. L. Heath, and G. Wilemski (unpublished).

[5] M. H. Schwartz and R. P. Andres, J. Aerosol Sci. **7**, 281 (1976).

[6] National Institute of Standards and Technology, Cold Neutron Research Facility, Gaithersburg, Maryland, NG3 and NG7 30-meter SANS Instruments Data Acquisition Manual, June, 1996.

[7] W. H. Press, S. A. Teukolsky, W. T. Vetterling, and B. P. Flannery, *Numerical Recipes in* FORTRAN: *the Art of Scientific Computing*, 2nd ed. (Cambridge University Press, Cambridge, England, 1992).